Stable and Efficient Coupling of High-Power Continuous-Wave Laser With Uncooled Anti-Resonant Hollow-Core Fibers With End Caps

Yulong Cui, Xinyu Ye, Jing Shi, Wei Huang, Zhiyue Zhou, Meng Wang, Zilun Chen, and Zefeng Wang

Abstract—Hollow-core fibers provide an ideal environment for the interaction of a laser and gases; however, achieving stable and efficient coupling of a high-power laser is one of the key problems to be solved. Here, we study stable and efficient coupling of a high-power continuous-wave fiber laser with anti-resonant hollow-core fibers spliced with end caps. By optimizing the splicing process, a maximum laser power of 460 W was injected and 356.5 W was outputted under uncooled conditions, realizing a total transmission efficiency of approximately 77.5%. A test of more than 1 h showed the stability of this a coupling method. A few other important characteristics, such as the Fresnel reflection of the end caps and the influence of the end caps on the transmission beam quality, were measured and examined. This study opens new opportunities for stable and highly efficient coupling of high-power lasers with hollow-core fibers, which is significant for their applications in many other fields besides high-power fiber gas lasers, such as high-power laser delivery and liquid lasers in hollow-core fibers.

Index Terms—Hollow-core fibers, end caps, high power transmission, coupling methods.

I. INTRODUCTION

HOLLOW-core fibers (HCFs) have generated significant attention because of their high damage threshold, low nonlinearity, and ideal environment for the interaction of a laser and gases [1]. Their hollow core structures allow HCFs to guide light in air. By sealing HCFs and filling their cores with different types of gases, a novel class of lasers called fiber gas lasers (FGLs) has emerged. FGLs combine the advantages of

traditional gas lasers and fiber lasers, which have the potential to emit higher power and longer wavelengths than fiber lasers. In the past decade, significant progress has been made in FGLs [2]–[15]. Thus far, although various laser wavelengths from the visible to the mid-infrared have been demonstrated, the output laser power is only at the watt level. One main cause is that the coupling of the pump with the core of an HCF that is sealed by gas cells has an almost free space structure, and the rubber plugs used in the gas cells for sealing are deformed at high power. This influences both the coupling efficiency and stability. Therefore, studying stable and efficient coupling methods is important for high-power FGLs.

Although efficient laser coupling of several hundred watts without cooling [16] and at the kilowatt level with water cooling [17] has been demonstrated for high-power laser delivery using HCFs, the coupling is not sufficiently stable for long-term operation. Several attempts have been made to develop all-fiber structures for low-loss coupling, from solid-core fibers to HCFs. The most direct method is splicing, in which the main loss originates from the mode field mismatch of these two types of fibers. For ordinary photonics crystal fibers (PCFs), whose mode fields are relatively close to those of solid-core fibers, splicing is a feasible method. In 2005, an all-fiber gas cavity based on gas-filled hollow-core PCFs was reported, and the loss of splicing was approximately 1–2 dB, which was mainly due to the refractive index and mode field mismatch [18]. The loss of other methods that splice directly is approximately 2 dB, mainly because the mode fields of single-mode fibers (SMFs) are unsuitable for those of HCFs [19]. For large mode-area HCFs, the mode field diameters are typically tens of microns, which are much longer than those of SMFs. In splicing, there is a direct significant loss due to the mismatch of the mode fields. We previously proposed a method in which a tapered SMF was inserted into the core of an HCF [20]–[22]. By tapering the SMFs, the mode field diameters of the SMFs reached a maximum as the tapered diameter decreased. However, owing to the large mode fields of the HCFs used, which were twice to thrice greater than that of the tapered fibers, the lowest coupling loss was approximately 2 dB [20]. For the HCFs in which the mode field was relatively suitable, the coupling efficiency could be above 90% [22]; therefore, our proposed method is suitable
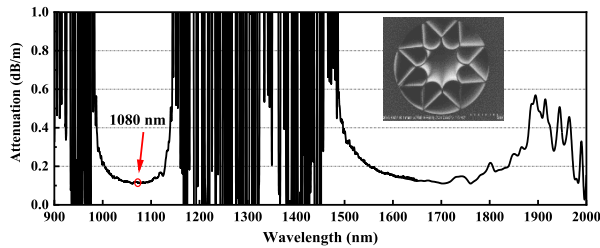
Fig. 1. Transmission loss of HCF used for splicing. Red arrow and circle represent pump wavelength. Inset: cross-section electronic micrograph of HCF.
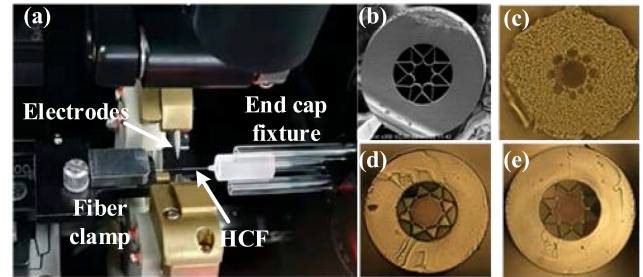

Fig. 2. (a) Image of splicing process. (b) Cross-section view of unheated HCF. Cross-section views of HCF at (c) relatively high temperature, (d) suitable temperature, and (e) relatively low temperature.

for HCFs with mode field diameters of less than 30 μm. Recently, a new two-step reverse tapering approach achieved low-loss coupling between SMFs and ultra-large mode-area PCFs in that the splicing loss was only 0.23 dB [23]. By reverse tapering the SMFs first and subsequently thermally expanding their core, mode field matching of the SMFs and the PCFs was achieved. Using the same method, a low loss of 0.88 dB was achieved for the two joints along an SMF/HCF/SMF [24]. Moreover, splicing between an HCF and a gain fiber was demonstrated, and a 90.4% efficiency was achieved [25]. At present, all coupling methods described above are suitable at low power levels; however, they are very difficult for high-power applications in FGLs. Recently, we proposed and preliminarily studied a new coupling method using end caps [26], which could promote the development of high-power FGLs.

In this study, we investigated in detail the performance of laser coupling with an anti-resonant HCF with an end cap. By optimizing the splicing process, a maximum laser power of 356.5 W was achieved at the output end when 460 W was injected, corresponding to a total transmission efficiency of approximately 77.5%. In addition, the characteristics of temperature increase, power stability, Fresnel reflection, and influence on the beam quality were studied and examined in detail. The research results validated that the coupling method using an end cap is stable and highly efficient for the HCF, where the end cap not only raises the coupled laser power but also seals the HCF as a cavity. This study provides an effective method for realizing high-power FGLs.

II. FABRICATION OF ANTI-RESONANT HCF WITH END CAP

In this study, the HCF used for splicing with an end cap is a type of ice-cream anti-resonant HCF. It has a core diameter of approximately 46 μm and a cladding diameter of approximately 280 μm, and the cross-section of the HCF is shown in the inset of Fig. 1. The core is surrounded by eight ice-cream capillaries forming an anti-resonant area, which contributes two transmission bands of the HCF from 1000 to 1100 nm and 1500 to 1900 nm, as shown in Fig. 1. The used wavelength lies in the first transmission band of the HCF, and the loss is approximately 0.12 dB/m.

A large-diameter splicing system is used as the splicing apparatus to splice the HCF and the end cap. An image of the splicing process is shown in Fig. 2(a). In the figure, the end cap is on the right side; it is composed of an all-silica material and rarely absorbs the input laser. The total length of the end cap is 20 mm

and the maximum diameter of the end cap is 8.2 mm; this design is sufficient when a Gaussian beam, which can reduce the power density, is transferred to the output end. In addition, at the wider end, an antireflection coating of 1080 nm is coated. At the other end of the end cap, a small cone with a minimum diameter of 1 mm is designed, for lowering the temperature when splicing, which prevents severe destruction of the HCFs. At the left side is the HCF, and to ensure the results of the splicing, an HCF must have a smooth surface. A Fujikura CT-102 fiber cleaver is used to cleave the HCF to ensure that the angle of the surface of the HCF is less than 0.5°. Before the splicing process, the HCF is fixed by a fiber clamp and the end cap is fixed by a self-made clamp composed of three glass tubes. An adjustment is needed to ensure that the center of the HCF is aligned with the center of the end cap. Three electrodes are used to heat the end cap to a molten state evenly, and subsequently, the electrodes shifted away by a short distance, and the waste heat is used to splice the HCF and the end cap.

The hollow-core structure is a characteristic of the HCF; however, it also leads to significant difficulty in the fabrication of the HCF end cap. During the splicing process, the HCF is in direct contact with the end cap in the molten state, and a high temperature can destroy its hollow-core structure, particularly for tubes with a thin wall thickness. Therefore, controlling the heating temperature is important. In addition, we typically shift the electrodes away after heating the end cap to the molten state, and use the waste heat to splice the HCF and the end cap to ensure minimal damage to the HCF cladding. Fig. 2(b)–(e) show cross-section views of the HCF with and without splicing. Fig. 2(b) presents the unheated cross-section, where the cladding has a completely negative curvature structure. When the temperature is relatively high, the cladding structure is destroyed, as shown in Fig. 2(c). The mode field and the transmission band are expected to change owing to the disappearance of the cladding, which is not a good splicing state. Fig. 2(d) shows that when the temperature is suitable, despite the negative curvature being destroyed, the cladding structure is maintained and the length of the collapse is short. Although the mode field will change slightly in this case, the combination of the lenses can be modified to maintain the coupling efficiency, which can affect the light transmission. Fig. 2(e) shows that when the temperature is relatively low, although the complete cladding structure and the negative curvature are maintained, the HCF and the end cap
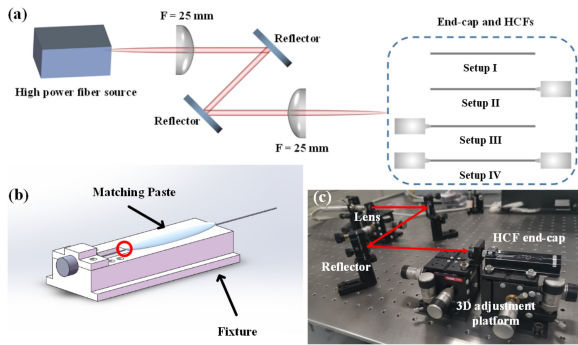
Fig. 3. (a) Experimental setup of system for testing efficiency of HCF end cap. Structures that need to be tested are surrounded by dotted lines: Setup I, HCF only; Setup II, HCF and end cap as output end; Setup III, HCF and end cap as the input end; and Setup IV, HCF and end caps at both ends. (b) Structure of fixture of HCF end cap. (c) Image of experimental system. Red arrows show direction of light.

Fig. 4. Total efficiency and output power variation with incident power. (a)–(d) correspond to Setups I–IV, respectively.

weakly stick to each other. Thus, an extremely small force will be sufficient to separate the HCF and the end cap. Considering the above three structures after splicing, the structure corresponding to Fig. 2(d) is the desired structure.

III. EXPERIMENT OF HIGH-POWER LASER COUPLING WITH ANTI-RESONANT HCF WITH END CAP

A. Experimental Setup

Fig. 3(a) shows the testing system used for obtaining the efficiency of the HCF end cap. The laser source used is a high-power fiber laser that can emit over several hundred watts power at 1080 nm. The output end is the fiber end cap of a 20/400 solid-core fiber. Two plano-convex lenses with a focal length of 25 mm are used to convert the mode field, and two reflectors with high reflectivity (99.5%) are used to change the direction of the light and improving the coupling of the light with the HCF. The core diameter of the used HCF is 46 μm, and based on the principle of mode field matching and tests of several lens combinations, the above two lenses are suitable for high coupling efficiency. In the figure, the structure surrounded by dotted lines is measured under different conditions: no end cap, one end cap at the input or output end, and end caps at both ends. A 1-m-long HCF is used, and the whole fiber is straightened. The HCF end cap is fixed by a fixture design, as shown in Fig. 3(b). Because the anti-resonant HCF is a type of leaky fiber, an area where the cladding of the HCF and the fixture of the end cap contact, as indicated by a red circle, suffers from light leakage, which leads to heat accumulation. The matching paste is applied evenly near the heating area, as shown in the figure, and the temperature in this area is remarkably reduced, which can also reduce the temperature of the coating. Fig. 3(c) shows an image of the experimental system, where the lenses, reflectors, and fixture of the HCF end cap are set on a three-dimensional adjustment platform for easy adjustment of the coupling.

B. Experimental Results

Experiments were conducted under the four conditions shown in Fig. 3(a). The power characteristics and the efficiency curves
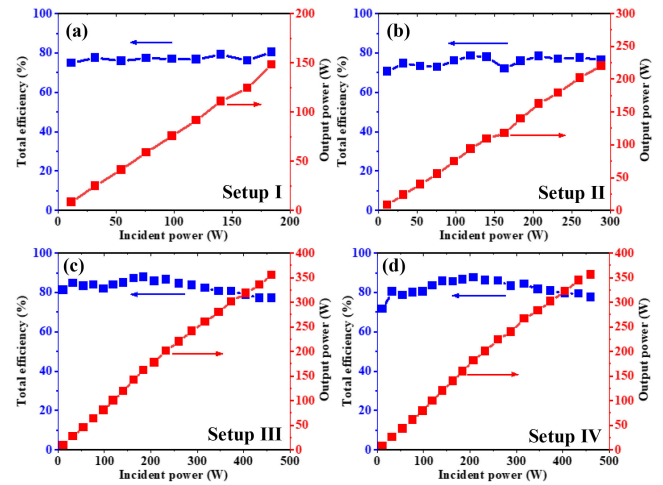
are presented in Fig. 4. The incident power is the power of the high-power fiber source output, and the output power is measured at the output end of the HCF. The result without the end-cap is shown in Fig. 4(a); the total efficiency is approximately 80.4%, of which the total loss includes the loss of the lenses and reflectors, coupling loss, and loss of the HCF. Among these, the loss of the lenses and reflectors is approximately 0.3 dB, loss of the HCF we used is 0.12 dB/m at 1080 nm, and loss of the 1-m-long HCF is 0.12 dB, and the coupling efficiency is estimated as 88.6%. Because the increment in the incident power is above 200 W, the input end of the HCF is destroyed, possibly because it is fixed on the fixture by only a foil tape. Moreover, significant energy is focused on the front of the HCF, and the heat accumulation at the input end may cause high temperature of the HCF as Fig. 5 shows. The suspended part of HCF may change its position without the support of the clamp because of the heat and the focus of the pump changed its position from the core to the thin capillary wall or the cladding, which destroys the HCF. Thus, high-power coupling from the free space to the HCF is difficult.

After splicing of the HCF and the end cap, HCF end cap was placed at both the input and output ends to measure the effect of the end cap, and the test results are shown in Fig. 4(b) and (c). Fig. 4(b) shows the results of the case in which the HCF end cap is at the output end, and Fig. 4(c) displays those when it is at the input end. The total efficiencies % under the two conditions are 76.5% and 77.1%, respectively. When the HCF end cap is set as the output end, similar to the experiment of the HCF without any end cap, it is not destroyed under a 250-W input power. However, compared to the Fig. 4(a) case, higher input power cannot be withstood to protect the HCF. In contrast, when the HCF end cap is set at the input end, it also plays a role in fixing the HCF, which can bear over 450 W of power under an uncooled system. The HCF with one end cap has a significant effect, as shown above, and when the other end is also spliced with an end cap, a cavity is formed. The test results are shown in Fig. 4(d). The total efficiency is approximately 77.5%, and when the maximum incident power is 460 W, the maximum output
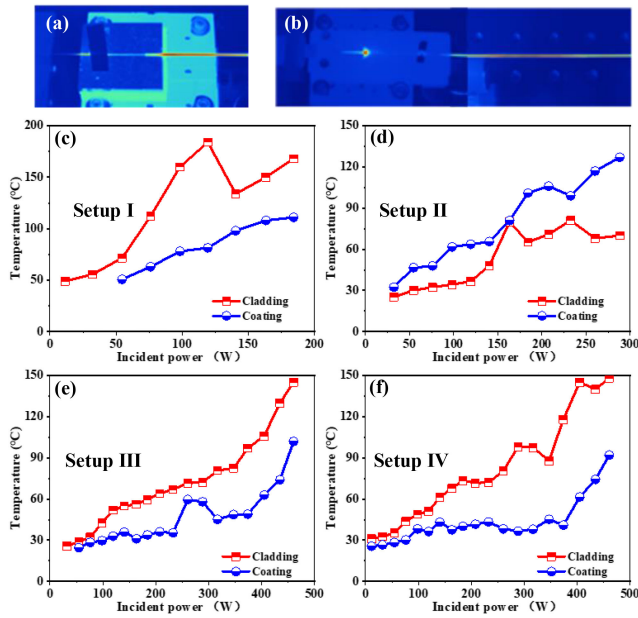
Fig. 5. (a) Thermal image of HCF without end cap. (b) Thermal image of HCF with end cap. (c)–(f) Temperature of cladding and coating versus incident power corresponding to Setups I–IV.
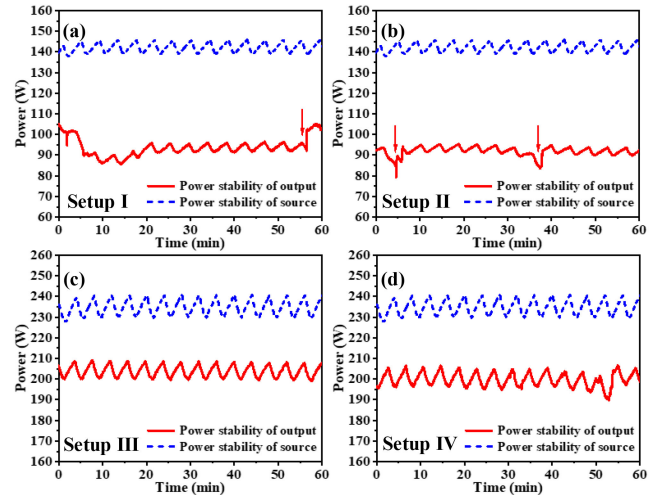

Fig. 6. Power stability of output and source, where dotted line represents source and straight line represents output. (a)–(d) correspond to Setups I–IV.

power is 356.5 W. Under the three conditions after splicing with an end cap, the total efficiency is lower than that without an end cap by approximately 3%, which is the Fresnel reflection of the end cap.

Among the four conditions, Fig. 4(a) and (b) correspond to the conditions that are directly input by the HCF, and without the protection of an end cap, the HCF is easily destroyed owing to the deformation caused by the heat accumulation. Although the condition corresponding to Fig. 4(b) has a higher input power than that for Fig. 4(a), it is an unstable coupling method. However, if the end cap is at the input end, a higher power can be injected into the HCF. The end cap plays a role in protecting and fixing the HCF. From the power characteristics, using an HCF end cap is a good method for high-power coupling.

Under uncooled system, the temperature of the HCF is an important factor for the stability of the system, to keep the system running safely and stably for a period time, the monitor of the temperature is necessary. An infrared thermal imager from Fluke is used to measure the temperature of the system. For the HCF input, there are two hot positions as Fig. 5(a) shows, the first point is the front of the cladding which is caused by the leakage light, the second position is the front of the coating. And for the HCF with end-caps at both ends, as Fig. 5(b) shows, there are also two hot positions, one is the touching point between the HCF and the fixture and the other is the front of the coating. And at the output end, there is nearly no heat accumulation.

Fig. 5(c)–(f) show that the monitored temperatures of the hot positions vary with the incident power. In addition to the conditions corresponding to Fig. 5(d), a matching paste is added, which allows the temperature of the coating to be higher than that of the cladding, as shown in Fig. 5(d). Because the HCF is a type of leaky fiber, its temperature is much higher than that of the solid-core fiber because of the leakage of light.

However, the core of the HCF is air and its damage threshold is higher than that of the solid-core fiber; in addition, the high temperature may be the surface temperature. We consider 100 °C as a safe temperature when increasing the power. In Fig. 5(c), the temperature is slightly higher than 100 °C when the input power is 100 W. A notable drop in the temperature at approximately 150 W is due to the manual adjustment of the coupling. As shown in Fig. 5(d), by shortening the distance that the HCF reaches out the fixture, the temperature is lowered compared to that shown in Fig. 5(c), and a higher input power is achieved. Without the matching paste, the temperature of the coating is higher than 100 °C. As shown in Fig. 5(e) and (f), after splicing with the end cap, the temperature is relatively lower than those in Fig. 5(c) and (d) at the same input power. When the power is less than 400 W, the temperature is still lower than 100 °C, and the temperature increases rapidly over 400 W, owing to the reduction in total efficiency. The reduction may be caused by two reasons. One is that as the power increased, the spot diameter of the pump increased, less power was coupled into the core of HCF. Another is that the temperature of the lens gets high [16], which change the focus length of the lenses, therefore the efficiency gets lower. As the input power reaches 460 W, the increase in the input power is stopped to protect the system, and the temperature of the cladding is as high as 150 °C. The dropping points in Fig. 5(e) are caused by manual adjustment.

The power stability of the source and output is tested, and the results are shown in Fig. 6. The blue dotted line represents the power stability of the fiber source. Throughout the entire testing time of 1 h, the power presents a periodic rise and fall, which is mainly because the operation period of the cooling system for the laser source starts, the temperature of the source starts to decrease and the power starts to drop. From Fig. 6(a) and (b), there are some points at which the power drops because of the heat accumulation, which is similar to the conditions in [16]. The red arrows represent the points manually adjusted. In these two conditions, after a few moments of stable operation, the coupling state is changed by the heat accumulation, and
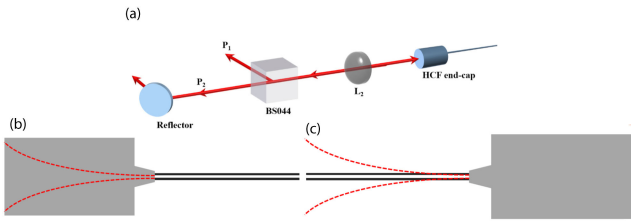
Fig. 7. (a) Schematic of test for Fresnel reflection. (b) Fresnel reflection at input end. (c) Fresnel reflection at output end.

manual adjustment is required. However, under the conditions in Fig. 6(c) and (d), the power is more stable, and the power is simply changed along with the trend of the laser source. This is because the end cap is fixed, and the HCF is not easily deformed. Compared with direct coupling with the HCF, splicing with an end cap supports a more stable method to couple higher power with the HCF.

IV. DISCUSSION

A. Fresnel Reflection of End Cap

The splicing between the HCF and the end cap is different from the splicing between the solid-core fiber and the end cap; because there is an interface between the silica and the air, a Fresnel reflection exists. To measure the Fresnel reflection of the HCF end-cap, a non-polarizing beam splitter cube from Thorlabs (BS044) is set between the second reflector and the second lens; a schematic of the testing process is shown in Fig. 7(a). Before use, the real (R:T) split ratio measured is 5:95 in the reverse direction. The back-forward light is separated into two, P_1 and P_2, where P_1 is measured by a power meter, and P_2 is calculated based on the split ratio of the splitter cube.

Using the method above, the Fresnel reflection is obtained. For the condition without an end cap, there is no Fresnel reflection. Under the condition in which the end cap is at the output end, the Fresnel reflection is approximately 1.5%, and under the condition in which it at the input end, the Fresnel reflection is approximately 3.5%. Two conditions have a difference of reflective surfaces. As shown in Fig. 7(b) and (c), when the end cap is at the input end, the reflection surface is the one that in the silica, whereas when the end cap is at the output end, the reflection surface is the one that is directly heated by the electrodes. The reflected light will pass the collapse area caused by the fabrication with end cap. Therefore, not all reflected light can return to BS044, which caused the lower reflectivity of the output end cap. For the HCF with end caps at both ends, the measured Fresnel refection is 3.9%.

B. Influence on Beam Quality

M^2 is a common parameter used to measure laser beam quality. To further investigate the influence of the end cap on the beam quality, M^2 of the output was measured by a laser quality monitor from PRIMES. Fig. 8(a) shows the M^2 of the laser source at a power level of 1500 W, which is measured as 1.17, and it is nearly stable at any power level below 1500 W. Fig. 8(a) also shows the beam profile of the waist. The HCF has good transmission
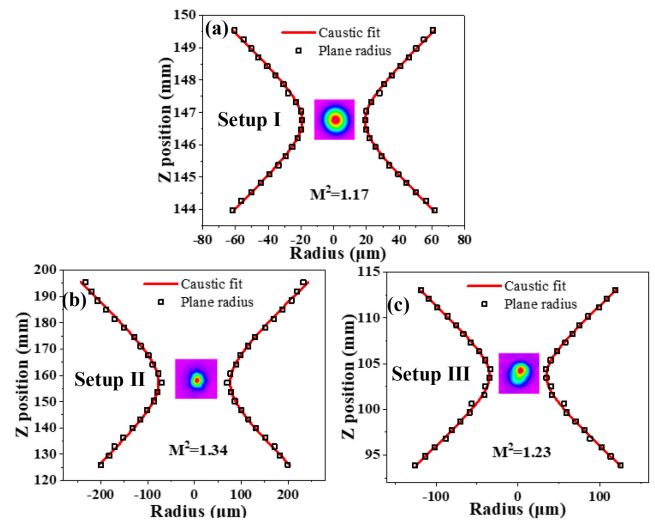

Fig. 8. Measured M^2 of (a) laser source, (b) fiber output of Setup III, and (c) end cap output of Setup IV. Inset: beam profile of waist.
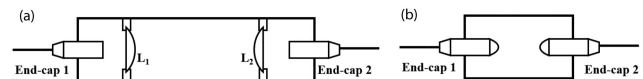

Fig. 9. Layout of coupling device based on HCF end cap.

characteristics, and the high-order mode has a higher loss than the low-order one, and through a distance of transmission, there is almost a fundamental mode in the HCF. Here, we measured the M^2 under the two conditions corresponding to Setups III and IV, as shown in Fig. 8(b) and (c), respectively. At the output power level of 200 W, the M^2 of Setups III and IV are 1.34 and 1.23, and from the beam profile of the waist, there is some light surrounding the central beam owing to the distinct shape of the HCF. Through the negative curvature, the beam is limit in the core, but from the interval of the negative curvature, there is also some light, which will lead to the measuring error of the M^2. Like the inset picture in Fig. 8(b), the measured radius is larger than the real value, and the measured M^2 is quite large. In comparison, in the inset picture in Fig. 8(c), the surrounding light is weakened by the destruction of the negative curvature; therefore, the measured M^2 is lower than that of Setup III.

C. Design of Integrated End-Cap Coupling Device

Based on the experimental results presented in Section III, the coupling method of using HCF end caps is an efficient method with the ability to transmit power of several hundred watts. One disadvantage is that the system is not sufficiently compact. A compact coupling device based on an HCF end cap is required. The layout of the coupling device is shown in Fig. 9. One method is shown in Fig. 9(a), where End cap 1 is that splicing with the solid-core fiber and End cap 2 is that splicing with the HCF, and both end caps are encapsulated in a shell. Two lenses are used to match the mode field. All devices are designed for miniaturization. Using this device, the input end can splice directly with the solid-core fiber, which is more convenient and stable than present conditions. Another method

is shown in Fig. 9(b), where the front end of the end cap is melted into a ball, which plays a role in the lens, and both end caps are encapsulated directly [27], which can reduce the volume of the device significantly.

V. Conclusion

The splicing between an HCF and an end cap provides a new method for high-power coupling of an SMF and an HCF. The end cap can play roles of both fixing the HCF and protecting the end face of the HCF. In this study, more detailed research on an HCF end cap was conducted. By further optimizing the splicing process, an output power of over 356.5 W with an uncooled system was delivered in the HCF under a maximum input power of 460 W with a total efficiency of 77.5%. By the achieved power stability and monitoring of the temperature, the HCF end cap is proven to be a stable method for long-term operation.

If a cooling system is added, high-power delivery will be allowed in the HCF for transmission. However, the Fresnel reflection is still a difficult problem that needs to be solved. Although splicing the HCF with an end cap of an inclined plane may be an effective method, it is difficult to realize. We consider another new method in which an end-cap and a lens are integrated as a miniaturized device, such as a fiber isolator, which will increase the stability of the system and simplify the structure. Based on this research, an HCF end cap is proven to be an effective device for HCFs, providing a route for the development of high-power FGLs

Acknowledgment

References

[1] P. Russell, P. Hölzer, W. Chang, A. Abdolvand, and J. C. Travers, "Hollow-core photonic crystal fibres for gas-based nonlinear optics," *Nat. Photon.*, vol. 8, no. 4, pp. 278–286, 2014.

[2] F. Benabid, "Stimulated Raman scattering in hydrogen-filled hollow-core photonic crystal fiber," *Science*, vol. 298, no. 5592, pp. 399–402, 2002.

[3] A. V. Gladyshev *et al.*, "4.4 μm Raman laser based on hollow-core silica fibre," *Quantum Electron.*, vol. 47, no. 5, pp. 491–494, 2017.

[4] A. V. Gladyshev *et al.*, "2.9, 3.3 and 3.5 μm Raman lasers based on revolver hollow-core silica fiber filled by H_2/d_2 gas mixture," *IEEE J. Sel. Top. Quantum Electron.*, vol. 24, no. 3, May/Jun. 2018, Art. no. 0903008.

[5] Z. Li, W. Huang, Y. Cui, and Z. Wang, "Efficient mid-infrared cascade Raman source in methane-filled hollow-core fibers operating at 2.8 μm," *Opt. Lett.*, vol. 43, no. 19, pp. 4671–4674, 2018.

[6] L. Cao, S. Gao, Z. Peng, X. Wang, and P. Wang, "High peak power 2.8 μm Raman laser in a methane-filled negative-curvature fiber," *Opt. Exp.*, vol. 26, no. 5, pp. 5609–5615, 2018.

[7] W. Huang, Y. Cui, Z. Li, Z. Zhou, and Z. Wang, "1.56 μm and 2.86 μm Raman lasers based on gas-filled anti-resonance hollow-core fiber," *Chin. Opt. Lett.*, vol. 16, no. 7, 2019, Art. no. 071406.

[8] M. S. Astapovich, A. V. Gladyshev, M. M. Khudyakov, A. F. Kosolapov, M. E. Likhachev, and I. A. Bufetov, "Watt-level nanosecond 4.42-μm Raman laser based on silica fiber," *IEEE Photon. Technol. Lett.*, vol. 1, no. 31, pp. 78–81, Jan. 2019.

[9] A. M. Jones, A. V. V. Nampoothiri, A. Ratanavis, T. Fiedler, and W. Rudolph, "Mid-infrared gas filled photonic crystal fiber laser based on population inversion," *Opt Exp.*, vol. 19, no. 3, pp. 2309–2316, 2011.

[10] Z. Wang, W. Belardi, F. Yu, W. J. Wadsworth, and J. C. Knight, "Efficient diode-pumped mid-infrared emission from acetylene-filled hollow-core fiber," *Opt. Exp.*, vol. 22, no. 18, pp. 21872–21878, 2014.

[11] M. R. A. Hassan, F. Yu, J. Wadsworth, and J. C. Knight, "Cavity-based mid-IR fiber gas laser pumped by a diode laser," *Optica*, vol. 3, no. 3, pp. 218–221, 2016.

[12] M. Xu, Y. Fei, and K. Jonathan, "Mid-infrared 1 w hollow-core fiber gas source," *Opt. Lett.*, vol. 42, no. 20, pp. 4055–4058, 2017.

[13] Z. Zhou *et al.*, "High-power tunable mid-infrared fiber gas laser source by acetylene-filled hollow-core fibers," *Opt. Exp.*, vol. 26, no. 15, pp. 19144–19153, 2018.

[14] Y. Cui *et al.*, "4.3 μm fiber laser in CO_2 fibers," *Optica*, vol. 6, no. 8, pp. 951–954, 2019.

[15] F. B. A. Aghbolagh *et al.*, "Mid IR hollow core fiber gas laser emitting at 4.6 um," *Opt. Lett.*, vol. 44, no. 2, pp. 383–386, 2019.

[16] X. Zhu *et al.*, "Delivery of CW laser power up to 300 watts at 1 μm by uncooled low-loss antiresonant hollow-core fiber," *Opt. Exp.*, vol. 29, no. 2, pp. 1492–1501, 2020.

[17] S. H. Drich *et al.*, "Scalability of components for kW-level average power few-cycle lasers," *Appl. Opt.*, vol. 55, no. 7, pp. 1636–1640, 2016.

[18] F. Benabid, F. Couny, J. Knight, T. Birks, and P. Russell, "Compact, stable and efficient all-fibre gas cells using hollow-core photonic crystal fibres," *Nature*, vol. 434, no. 7032, pp. 488–491, 2005.

[19] P. S. Light, F. Couny, and F. Benabid, "Low optical insertion-loss and vacuum-pressure all-fiber acetylene cell based on hollow-core photonic crystal fiber," *Opt. Lett.*, vol. 31, no. 11, pp. 2538–2540, 2006.

[20] Y. Cui, Z. Zhou, W. Huang, Z. Li, and Z. Wang, "Quasi-all-fiber structure CW mid-infrared laser emission from gas-filled hollow-core silica fibers," *Opt. Laser Technol.*, vol. 121, 2019, Art. no. 105794.

[21] W. Huang, Y. Cui, Z. Zhou, Z. Li, Y. Chen, and Z. Wang, "Towards all-fiber structure pulsed mid-infrared laser by gas-filled hollow-core fibers," *Chin. Opt. Lett.*, vol. 17, no. 9, pp. 68–71, 2019.

[22] W. Huang, Y. Cui, Z. Li, Z. Zhou, and Z. Wang, "Low-loss coupling from single-mode solid-core fibers to anti-resonant hollow-core fibers by fiber tapering technique," *Opt. Exp.*, vol. 27, no. 26, pp. 37111–37121, 2019.

[23] R. Yu, C. Wang, F. Benabid, K. S. Chiang, and L. Xiao, "Robust mode matching between structurally dissimilar optical fiber waveguides," *ACS Photon.*, vol. 8, no. 3, pp. 857–863, 2021.

[24] C. Wang *et al.*, "Ultralow-loss fusion splicing between negative curvature hollow-core fibers and conventional SMFs with a reverse-tapering method," *Opt. Exp.*, vol. 29, no. 14. pp. 22470–22478, 2021.

[25] C. Goel, H. Li, M. R. Abu Hassan, W. Chang, and S. Yoo, "Anti-resonant hollow-core fiber fusion spliced to laser gain fiber for high-power beam delivery," *Opt. Lett.*, vol. 46, no. 17, pp. 4374–4377, 2021.

[26] J. Shi *et al.*, "All-fiber gas cavity based on anti-resonant hollow-core fibers fabricated by splicing with end caps," *Photonics*, vol. 9, no. 8, 2021, Art. no. 371.

[27] X. Zhou, Z. Chen, Z. Wang, and J. Hou, "Monolithic fiber end cap collimator for high-power free-space fiber–fiber coupling," *Appl. Opt.*, vol. 55, no. 15, pp. 4001–4004, 2016.